

Long-term evolution of orbits about a precessing oblate planet:

3. A semi-analytical and a purely numerical approach.

PinGur 1

Faculty of Aerospace Engineering, Technion, Haifa 32000 Israel

email: pgur 1@technion.ac.il ,

Valery Lainey

Observatoire Royal de Belgique, Avenue Circulaire 3, Bruxelles 1180 Belgium ,

IMCCE/Observatoire de Paris, UMR 8028 du CNRS, 77 Avenue Denfert-Rochereau, Paris 75014 France

email: Valery.Lainey @ in.oe.fr ,

and

Michael E. Fromm

US Naval Observatory, Washington DC 20392 USA

email: m.e @ usno.navy.mil

February 7, 2020

Abstract

Construction of an accurate theory of orbits about a precessing and nutating oblate planet, in terms of osculating elements defined in a frame associated with the equator of date, was started in E. Fromm & Goldreich (2004) and E. Fromm (2004b, 2005, 2006). Here we continue this line of research by combining that analytical machinery with numerical tools. Our model includes three factors: the J_2 of the planet, its nonuniform equinoctial precession described by the Colombo formalism, and the gravitational pull of the Sun. This semi-analytical and semi-numerical theory, based on the Lagrange-type planetary equations for the Keplerian elements, is then applied to dimensions on very long time scales (up to 1 billion of years). In parallel with the said semi-analytical theory for the Keplerian elements defined in the co-precessing equatorial frame, we have also carried out a completely independent, purely numerical, integration in a fixed inertial Cartesian frame. The results agree to within $10^{-3} - 10^{-2}$ (from 0.3%, for near-polar orbits, through 1.3% for near-equatorial ones), for over 20 Myr, thus demonstrating the applicability of our semi-analytical model over long

We use the term 'precession' in its general meaning, which includes any change of the instantaneous spin axis. So generally defined precession embraces the entire spectrum of spin-axis variations { from the polar wander and nutations through the Chandler wobble through the equinoctial precession.

tim escales. This will enable us to employ the semi-analytical model at the further stages of the project, enriching this model with the tides and the planet's triaxiality. (Lainey, Efromsky & Gur 2007)

Another goal of this work was to make an independent check of whether the equinoctial precession of Mars, as predicted for a rigid Mars, could have been sufficient to repel the orbits away from the equator. The answer to this question, in combination with our knowledge of the current position of Phobos and Deimos, will help us to understand whether this precession could indeed have always been as large as predicted or whether it ought to have been less in the past. It has turned out that, both for high and low initial inclinations, the orbit inclination reckoned from the precessing equator of date is subject only to small variations (from about 10^3 deg, for near-equatorial satellites, to about 2 deg, for polar ones). This is an extension, to non-uniform equinoctial precession given by the Colombo model and to an arbitrary initial inclination, of an old result obtained by Goldreich (1965) for the case of uniform precession and a low initial inclination. Such "inclination locking", or the "Goldreich lock", means that an oblate planet can, indeed, afford a large equinoctial precession for billions of years, without repelling its near-equatorial satellites away from the equator of date: the satellite inclination oscillates but does not show a secular increase. Nor does it show secular decrease, a fact that is relevant to the discussion of the possibility of high-inclination capture of Phobos and Deimos.

1 Introduction

1.1 Statement of purpose

The goal of this paper is to explore, by two very different methods, inclination variations of a solar-gravity perturbed satellite orbiting an oblate planet subject to nonuniform equinoctial precession. This nonuniformity of precession is caused by the presence of the other planets. Their gravitational pull entails precession of the circum solar orbit of our planet; this entails variations of the solar torque acting on it; these torque variations make the planet's equinoctial precession nonuniform; and this nonuniformity, in its turn, influences the behaviour of the planet's satellites. This influence is feeble, and we trace with a great accuracy whether over huge spans of time it results in purely periodic changes in inclination or can accumulate to secular changes.

It should be emphasised that this work is but a small part of a larger project, the eventual goal whereof will be to build up a comprehensive tool for computation of long-term orbital evolution of satellites. The tool, in its final form, will contain the triaxiality, the tides, and the planet's precession. Building this tool, block by block, we are beginning with only three components { the planet's oblateness, the direct pull of the Sun on the satellite and the planet's precession. These phenomena bear a marked effect on the evolution of the orbit. In our subsequent publications, we shall incorporate more effects into our model { J_2^2 , the triaxiality, and the tides.

1.2 Motivation

One motivation for this work stems from our intention to carry out an independent check of whether Mars could have performed, through all of its past history, the same large equinoctial precession as it is performing at present. Such a check is desirable because the current theory of equinoctial precession, based on the Colombo model, incorporates, as any theory, certain approximations. First, the Colombo equation is derived under the assertion that the planet is rigid and that it is always in its principal spin state, the angular momentum vector staying parallel

to the angular-velocity one. Second, this description, being only a model, ignores the possibility of planetary catastrophes that might have altered the planet's spin mode. Fortunately, in the case of Mars there may exist a model-independent test that may bring restrictions on the amplitude of the equinoctial precession in the past. This test is based on the necessity to reconcile the variations of spin with the present near-equatorial positions of Phobos and Deimos. The fact that both moons found themselves on near-equatorial orbits, in all likelihood, billions of years ago,¹ and that both are currently located within less than 2° degrees from the equator, is surely more than a mere coincidence. An elegant but sketchy calculation by Oldreich (1965) demonstrated that the orbits of initially near-equatorial satellites remain close to the equator of date for as long as some simplifying assumptions remain valid. As explained in Efron sky (2004b, 2005), these assumptions are valid over time scales not exceeding 100 million years, while at longer times a more careful analysis is required. Its goal will be to explore the limits for the possible secular drift of the satellite orbits away from the evolving equator of date. Through comparison of these limits with the present location of the Martian satellites, we shall be able to impose restrictions upon the long-term spin variations of Mars. If, however, it turns out that near-equatorial satellites can, in the face of large equinoctial precession of the oblate primary, remain for billions of years close to the moving equator of date, then we shall admit that Mars' equator is likely to have precessed through billions of years in the same manner as it is doing now.

The second motivation for our study comes from the ongoing discussion of whether the Martian satellites might have been captured at high inclinations, their orbits having gradually approached the equator afterwards. While a comprehensive check of this hypothesis will need a more detailed model (one that will include Mars' triaxiality, the tidal forces, (Lainey, Efron sky & Gur 2007), and perhaps other perturbations (the first, rough sketch of this test can be carried out with only J_2 , the Sun, and the equinoctial precession taken into account. We perform such a rough check for a hypothetical satellite that has all the parameters of Deimos, except that its initial inclination is 89° .

1.3 Mathematical tools

The first steps toward the analytical theory of orbits about a precessing and nutating Earth were undertaken almost half a century ago by Brouwer (1959), Proskurin & Batrakov (1960), and Kozai (1960). This problem was considered, in application to the Martian satellites, by Oldreich (1965) and, in regard to a circum-lunar orbiter, by Bumberg, Evdokimova, & Kochina (1971). The latter two publications addressed the dynamics as seen in a non-inertial frame associated with the planet's equator of date. The analysis was carried out in terms of the so-called "contact" Kepler elements, i.e., in terms of the Kepler elements satisfying a condition different

¹ Phobos and Deimos give every appearance of being captured asteroids of the carbonaceous chondritic type, with cratered surfaces older than 10^9 years (Neverka 1977; Pang et al. 1978; Pollack et al. 1979; Tolson et al. 1978). If they were captured by gas drag (Burns 1978), this must have occurred early in the history of the solar system while the gas disk was substantial enough. At that stage of planetary formation, the spin of the forming planet would be perpendicular to the planet's orbit about the Sun (i.e., the obliquity would be small and the gas disk would be nearly coplanar with the planetary orbit. Energetically, a capture would likely be equatorial. This is most easily seen in the context of the restricted three-body problem. The surfaces of zero velocity constrain any reasonable capture to occur from directions near the inner and outer collinear Lagrange points (Szebehely 1967, Murray 1988), which lie in the equatorial plane. Also, a somewhat inclined capture would quickly be equatorialized by the gas disk. If the capture inclination is too high, the orbital energy is then too high to allow a long enough temporary capture, and the object would hence not encounter enough drag over a long enough time to effect a permanent capture (Murray 1988). Thus, Phobos and Deimos were likely (in as much as we can even use that term) to have been captured into near-equatorial orbits.

from that of osculation. Modelling of perturbed trajectories by sequences of instantaneous ellipses (or hyperbolae) parameterised with such elements is sometimes very convenient mathematically (Efroimsky 2002a,b; Newman & Efroimsky 2003; Efroimsky & Goldreich 2003, 2004). However, the physical interpretation of such solutions is problematic, because instantaneous conics defined by nonosculating elements are nontangent to the trajectory. Though over restricted time scales the secular parts of the contact elements may well approximate the secular parts of their osculating counterparts (Efroimsky 2004b, 2005), the cleavage between them may grow at longer time scales (Efroimsky 2006). This is the reason wherefore a practically applicable treatment of the problem must be performed in the language of osculating variables.

1.4 The plan

The analytical theory of orbits about a precessing oblate primary, in terms of the Kepler elements defined in a co-precessing (i.e., related to the equator of date) frame, was formulated in Efroimsky (2006) where the planetary equations were approximated through averaging some of their terms. This way, from the exact equations for osculating elements, approximate equations for their secular parts were obtained. We shall borrow those averaged Lagrange-type planetary equations, shall incorporate into them the pull of the Sun, and shall numerically explore their solutions. This will give us a method that will be semi-analytical and semi-numerical. We shall then apply it to a particular setting { evolution of a Martian satellite and its reaction to the long-term variations of the spin state of Mars. Our goal will be to explore whether the spin-axis variations predicted for a rigid Mars permit its satellites to remain close to the equator of date for hundreds of millions through billions of years. In case the answer to this question turns out to be negative, it will compel us to seek nonrigidity-caused restrictions upon the spin variations. Otherwise, the calculations of the rigid-Mars inclination variations will remain in force (and so will the subsequent calculations of Mars obliquity variations); this way, the theory of Ward (1973, 1974, 1979, 1982) will get a model-independent continuation.

2 Semi-analytical treatment of the problem

To understand the evolution of a satellite orbit about a precessing planet, it is natural to model it with elements defined in a coordinate system associated with the equator of date, i.e., in a frame co-precessing (but not co-rotating) with the planet. A transition from an inertial frame to the co-precessing one is a perturbation that depends not only upon the instantaneous position but also upon the instantaneous velocity of the satellite. It has been demonstrated by Efroimsky & Goldreich (2004) that such perturbations enter the planetary equations in a nontrivial way: not only they alter the disturbing function (which is the negative Hamiltonian perturbation) but also they endow the equations with several extra terms that are not parts of the disturbing function. Some of these nontrivial terms are linear in the planet's precession rate $\dot{\omega}$, some are quadratic in it; the rest are linear in its time derivative $\ddot{\omega}$. The inertial-forces-caused addition to the disturbing function (i.e., to the negative Hamiltonian perturbation) consists of a term linear and a term quadratic in $\dot{\omega}$. (See formulae (1) and (6) in Efroimsky (2006) or formulae (53–54) in Efroimsky (2004b, 2005).) The essence of approximation elaborated in Efroimsky (2006) was to neglect the quadratic terms and to substitute the terms linear in $\dot{\omega}$ and $\ddot{\omega}$ with their secular parts calculated with precision up to e^3 , inclusively.

2.1 Equations for the secular parts of osculating elements defined in a co-precessing reference frame.

We shall begin with five Lagrange-type planetary equations for the secular parts of the orbital elements, derived in E from sky (2004b, 2005):

$$\frac{da}{dt} = -2 \frac{e^2}{n} a \quad 1 - e^{1/2} ; \quad (1)$$

$$\frac{de}{dt} = \frac{5}{2} \frac{e^2}{n} e \quad 1 - e^{1/2} ; \quad (2)$$

$$\frac{d\Omega}{dt} = \frac{3}{2} \frac{n J_2}{(1 - e^2)^2} \frac{e^2}{a} \frac{5}{2} \cos^2 i \quad \frac{1}{2} + n \cot i \quad \frac{\cos i}{na^2 (1 - e^{1/2}) \sin i} \dot{h} \quad f \quad \frac{\partial f}{\partial i} \quad i ; \quad (3)$$

$$\begin{aligned} \frac{di}{dt} = & \quad 1 \cos \quad 2 \sin \\ & + \frac{\cos i}{na^2 (1 - e^{1/2}) \sin i} \dot{h} \quad f \quad \frac{\partial f}{\partial i} \quad i \quad \frac{1}{na^2 (1 - e^{1/2}) \sin i} \dot{h} \quad f \quad \frac{\partial f}{\partial i} \quad i ; \end{aligned} \quad (4)$$

$$\frac{d\Omega}{dt} = \frac{3}{2} n J_2 \frac{e^2}{a} \frac{\cos i}{(1 - e^2)^2} \frac{n}{\sin i} + \frac{1}{na^2 (1 - e^{1/2}) \sin i} \dot{h} \quad f \quad \frac{\partial f}{\partial i} \quad i ; \quad (5)$$

The number of equations is five, because one element, M_∞ , was excluded by averaging of the Hamiltonian perturbation and of the inertial terms emerging in the right-hand sides. In the equations, $n = G (m_{\text{primary}} + m_{\text{secondary}}) = a^3$, while $f(t; a; e; i; \Omega; M_\infty)$ is the implicit function that expresses the unperturbed two-body dependence of the position upon the time and Keplerian elements. Vector $\dot{\omega}$ denotes the total precession rate of the planetary equator (including all spin variations from the polar wander and nutations through the Chandler wobble through the equinoctial precession through the longest-scale spin variations caused by the other planets' pull), while $1; 2; 3$ stand for the components of $\dot{\omega}$ in a co-precessing coordinate system $x; y; z$, the axes x and y belonging to the equator-of-date plane, and the longitude of the node, Ω , being measured from x :

$$\dot{\omega} = 1 \hat{x} + 2 \hat{y} + 3 \hat{z} ; \quad \text{where} \quad 1 = \dot{I}_p ; \quad 2 = h_p \sin I_p ; \quad 3 = h_p \cos I_p ; \quad (6)$$

I_p ; h_p being the inclination and the longitude of the node of the equator of date relative to that of epoch, and dot standing for a time derivative. The quantity 3 is a component of $\dot{\omega}$ directed along the instantaneous orbital momentum of the satellite, i.e., perpendicular to the instantaneous osculating Keplerian ellipse. This component will be expressed with

$$3 = 1 \sin i \sin \dot{\omega} + 2 \sin i \cos \dot{\omega} + 3 \cos i ; \quad (7)$$

the unit vector

$$\mathbf{w} = \hat{x} \sin i \sin \hat{y} \sin i \cos \hat{z} \cos i \quad (8)$$

standing for the normal to the instantaneous osculating ellipse. Be mindful that the quantity ω is defined not as $d(\omega - w)/dt$ but as

$$\omega \sim \mathbf{w} = \omega_1 \sin i \sin \omega_2 \sin i \cos \omega_3 \cos i : \quad (9)$$

The quantity ω_n is a component pointing toward the ascending node of the satellite orbit relative to the equator of date:

$$\begin{aligned} \omega_n &= \omega_1 \sin i \cos i + \omega_2 \cos i \cos i + \omega_3 \sin i \\ &= I_p \sin i \cos i + h_p \sin I_p \cos i \cos i + h_p \cos I_p \sin i : \end{aligned} \quad (10)$$

Its time derivative taken in the frame of reference co-precessing with the equator of date is:

$$\begin{aligned} \dot{\omega}_n &= \omega_1 \sin i \cos i + \omega_2 \cos i \cos i + \omega_3 \sin i \\ &= I_p \sin i \cos i + h_p \sin I_p + h_p I_p \cos I_p \cos i \cos i + h_p \cos I_p h_p I_p \sin I_p \sin i : \end{aligned} \quad (11)$$

As shown in Efroimsky (2006), the \sim -dependent terms, emerging in equations (1 – 5), are expressed with

$$\begin{aligned} \dot{h} \sim f \frac{\partial f}{\partial i} i &= \\ \frac{a^2}{4} \omega_1 &= 2 + 3e^2 \cos i + 5e^2 (\cos i \cos 2! \sin i \sin 2! \cos i) + \\ \omega_2 &= 2 + 3e^2 \sin i + 5e^2 (\sin i \cos 2! + \cos i \sin 2! \cos i) + \\ \omega_3 &= 5e^2 \sin 2! \sin i \end{aligned} \quad (12)$$

$$\dot{h} \sim f \frac{\partial f}{\partial i} i = \frac{a^2}{2} (2 + 3e^2 (\omega_1 \sin i \sin \omega_2 \sin i \cos \omega_3 \cos i)) ; \quad (13)$$

$$\begin{aligned}
h \sim f \frac{\partial f}{\partial} i = & \\
\frac{a^2}{4} \underbrace{\sin i}_{-1} & 2 + 3e^2 \sin \cos i + 5e^2 (\cos \sin 2! + \sin \cos 2! \cos i) \\
+ \underbrace{\sin i}_{-2} & 2 + 3e^2 \cos \cos i + 5e^2 (\sin \sin 2! \cos \cos 2! \cos i) \\
\underbrace{2}_{-3} & 2 + 3e^2 2 \sin^2 i + 5e^2 \sin^2 i \cos 2! \quad (14)
\end{aligned}$$

To integrate equations (1 – 5), with expressions (12 – 14) inserted therein, we shall need to know, at each step of integration, the components of \sim and \sim .

2.2 Calculation of the components of \sim and \sim .

At each step of our integration, the components of \sim and \sim will be calculated in the Colombo approximation. Physically, the essence of this approximation is two-fold: first, the solar torque acting on the planet is replaced by its average over the year; and, second, the precessing planet is assumed to be always in its principal spin state. While a detailed development (based on the work by Colombo (1966)) may be found in the Appendix to E from sky (2006), here we shall provide a concise list of resulting formulae to be used.

The components of \sim are connected, through the medium of (6), with the inclination and the longitude of the node of the moving planetary equator, I_p and h_p , relative to some equator of epoch. These quantities and their time derivatives are connected with the unit vector \hat{k} aimed in the direction of the major-inertia axis of the planet:

$$\hat{k} = (\sin I_p \sin h_p; \sin I_p \cosh h_p; \cos I_p)^T : \quad (15)$$

This unit vector and its time derivative

$$\frac{d\hat{k}}{dt} = I_p \cos I_p \sin h_p + h_p \sin I_p \cosh h_p; \quad I_p \cos I_p \cosh h_p + h_p \sin I_p \sin h_p; \quad I_p \sin I_p^T; \quad (16)$$

depend, through the Colombo equation

$$\frac{d\hat{k}}{dt} = \hat{n} \hat{k} \hat{k} \hat{n}; \quad (17)$$

upon the unit normal to the planetary orbit,

$$\hat{n} = (\sin I_{orb} \sin h_{orb}; \sin I_{orb} \cos h_{orb}; \cos I_{orb})^T; \quad (18)$$

h_{orb} and I_{orb} being the node and inclination of the orbit relative to some fiducial fixed plane.

Hence, to find the components of \mathbf{h} , one must know the time evolution of h_p and I_p , which can be determined by solving a system of three differential equations (17), with h_{orb} and I_{orb} being some known functions of time. These functions may be computed via the auxiliary variables

$$q = \sin I_{\text{orb}} \sin \omega_{\text{orb}} ; \quad p = \sin I_{\text{orb}} \cos \omega_{\text{orb}} ; \quad (19)$$

whose evolution will be given by the formulae of Brouwer & van Woerkom (1950):

$$q = \sum_{j=1}^{X^1} N_j \sin s_j^0 t + \phi_j ; \quad (20)$$

$$p = \sum_{j=1}^{X^1} N_j \cos s_j^0 t + \phi_j ; \quad (21)$$

The following choice of the values of the amplitudes, frequencies, and phases will make equations (19–21) render h_{orb} and I_{orb} relative to the ecliptic plane of 1950:²

j	N_j	s_j^0 (arcsec=yr)	ϕ_j^0 (deg)
1	0.0084889	5.201537	19.43255
2	0.0080958	6.570802	318.05685
3	0.0244823	18.743586	255.03057
4	0.0045254	17.633305	296.54103
5	0.0275703	+ 0.000004	107.10201
6	0.0028112	25.733549	127.36669
7	0.0017308	2.902663	315.06348
8	0.0012969	0.677522	202.29272

The development by Brouwer & van Woerkom (1950) is limited in precision and, therefore, in the time span over which it remains valid. A more accurate and comprehensive development, which remains valid for (at least) tens of millions of years, was offered by Laskar (1988). At the future stages of our project, when developing a detailed physical model of the satellite motion, we shall employ Laskar's results. At this point we can save computer time by using the simple old formalism by Brouwer and van Woerkom, because our present goal is restricted: in the current paper, we are not yet building a consistent physical model, but are simply checking if the orbital averaging of the precession-caused terms is permissible at large time scales. Hence, for the purpose of this check we need a realistic, not necessarily real, scenario of the precession variations.

² This plane may well be chosen as crucial, because one may assume without loss of generality that at some initial, very distant, instant of time the satellite orbit belonged to that plane.

2.3 The Goldreich approximation

The above semi-analytical treatment not only yields plots of the time dependence of the mean elements but also serves as a launching pad for analytical approximations. For example, an assumption of a and e being constant, and a neglect of the \sim -dependent terms in (4–5), as well as of the term $n = \sin i$ in (5), gives birth to the Goldreich (1965) approximation:

$$\frac{da}{dt} = 0 ; \quad (22)$$

$$\frac{de}{dt} = 0 ; \quad (23)$$

$$\frac{di}{dt} = \begin{matrix} 1 \cos & 2 \sin \end{matrix} ; \quad (24)$$

$$\frac{d}{dt} = \frac{3}{2} n J_2 \frac{e^2}{a} \frac{\cos i}{(1 - e^2)^2} ; \quad (25)$$

$$\frac{d!}{dt} = \frac{3}{4} n J_2 \frac{e^2}{a} \frac{5 \cos^2 i}{(1 - e^2)^2} \frac{1}{\cos i \sin i} ? ; \quad (26)$$

the equinoctial precession being assumed uniform :

$$I_p = 0 \quad (27)$$

$$h_p = \quad (28)$$

$$_1 = 0 \quad (29)$$

$$_2 = 0 \quad (30)$$

$$_3 = h_p \cos I_p : \quad (31)$$

For the details of Goldreich's approximation see also subsection 3.3 in Efron (2005).

2.4 The Gravitational Pull of the Sun

Reaction of a satellite on the planetary-equator precession is, in a way, an indirect reaction of the satellite on the presence of the Sun and the other planets. Indeed, the pull of the other planets makes the orbit of our planet precess, which entails variations in the Sun-produced gravitational torque acting on our planet. These variations of the torque, in their turn, lead to the variable equinoctial precession of the equator, precession "felt" by the satellite. It would be unphysical to consider this, indirect effect of the Sun and the planets upon the satellite, without taking into account their direct gravitational pull. In this subsection, we shall take into account the pull of the Sun, which greatly dominates that of the planets other than the primary.

In what follows, m and m^0 will be the masses of the satellite and the Sun, correspondingly, \mathbf{r} and \mathbf{r}^0 will stand for the planetocentric positions of the satellite and the Sun, S will signify the angle between these vectors. Then the Sun-caused perturbing potential R_S , acting on the satellite, will assume the form of

$$R_S = G m^0 \frac{1}{\mathbf{r}^0 \cdot \mathbf{r} j} \frac{\mathbf{r}^0 \cdot \mathbf{r}}{r^0} = \frac{G m^0}{r^0} \frac{\mathbf{r}^0}{\mathbf{r}^0 \cdot \mathbf{r} j} \frac{r \cos S}{r^0} \quad (32)$$

This can be expanded in a usual manner over the Legendre polynomials of the first kind. Since $r^0 \ll r$, we shall take only the first term in the series:³

³This is justified since the next term in the Legendre series is about 2 orders of magnitude smaller than the potential of the precession.

$$R_s = \frac{G m^0}{r^0} \left(1 + \frac{r}{r^0} P_1(\cos S) + \frac{r^2}{r^0} P_2(\cos S) - \frac{r \cos S}{r^0} \right) \quad (33)$$

As the term $\frac{G m^0}{r^0}$ is not dependent of the satellite's elements, one has only to consider the restricted potential

$$R_s^1 = \frac{G m^0}{r^0} \left(\frac{r^2}{r^0} P_2(\cos S) - \frac{n^0 a^2}{2} - \frac{a^0}{r^0} (3 \cos^2 S - 1) \right); \quad (34)$$

n^0 and a^0 being the mean motion and the semi-major axis of the Sun.

To obtain the Lagrange-type equations for the third-body perturbation, we must first derive an expression for the angle S . To that end, define the directional cosines $\hat{P}^0 \hat{r}^0$ and $\hat{Q}^0 \hat{r}^0$, where \hat{r}^0 is a unit vector pointing from the planet toward the Sun, while \hat{P}^0 and \hat{Q}^0 are unit vectors of a perifocal coordinate system associated with the osculating orbital plane of the satellite, with \hat{P}^0 pointing to the instantaneous perapse and \hat{Q}^0 being orthogonal to \hat{P}^0 . Assuming that the planet's orbit about the Sun is circular, we arrive at

$$= \cos! \cos(M^0) \quad \cos i \sin! \sin(M^0); \quad (35)$$

$$= \sin! \cos(M^0) \quad \cos i \cos! \sin(M^0); \quad (36)$$

where M^0 is the mean anomaly of the Sun in the planetocentric frame. With aid of these relations, the angle S may be written down as

$$\cos S = \cos + \sin; \quad (37)$$

being the true anomaly of the satellite in the planetocentric coordinate system. Substituting (35) and (36) into (37), and averaging over the satellite's mean anomaly, we arrive at the Lagrange-type equations:

$$\frac{da}{d} = 0 \quad (38a)$$

$$\frac{de}{d} = 10e \frac{p}{1-e} \sin^2 i \sin 2! + (2 \sin^2 i) \sin 2! \cos 2^0 + 2 \cos i \cos 2! \sin 2^0 \quad (38b)$$

$$\frac{di}{d} = \frac{2 \sin i}{p \frac{1}{1-e}} \frac{n}{5e^2} \cos i \sin 2! (1 - \cos 2^0) - 2 + e^2 (3 + 5 \cos 2!) \sin 2^0 \quad (38c)$$

$$\begin{aligned} \frac{d!}{d} = & \frac{2}{p \frac{1}{1-e}} \frac{n}{4 + e^2} (5 \sin^2 i + 5 (\sin^2 i - e^2) \cos 2!) + 5 (e^2 - 2) \cos i \sin 2! \sin 2^0 \\ & + 5 (2 - e^2 \sin^2 i) \cos 2! - 2 - 3e + 5 \sin^2 i \cos 2^0 \end{aligned} \quad (38d)$$

$$\frac{d\tilde{}}{d} = \frac{2}{p \frac{1}{1-e}} \frac{n}{2 + e^2 (3 - 5 \cos 2!)} (1 - \cos 2^0) \cos i - 5e^2 \sin 2! \sin 2^0 \quad (38e)$$

In (38), we used the following set of notations:

$$n(t - \Omega) ; \quad = \frac{3m^0 a^3}{16M a^0} \quad (39)$$

$$\frac{16n}{3n^0} \quad 1 + \frac{M}{m^0} \quad (40)$$

$$\sim \quad \Omega ; \quad (41)$$

Ω being the mean longitude of the Sun in the planet's frame, and M being the mass of Mars.

An additional averaging can be performed over the motion of the planet about the Sun. Mathematically, this is the same as averaging over the motion of the Sun about the planet (in both cases averaging over Ω is implied). This will simplify (38) into

$$\frac{da}{dt} = 0 \quad (42a)$$

$$\frac{de}{dt} = 10e \frac{p}{1-e^2} n \sin^2 i \sin 2! \quad (42b)$$

$$\frac{di}{dt} = \frac{10e^2 \sin i}{p \frac{2}{1-e^2}} n \cos i \sin 2! \quad (42c)$$

$$\frac{d!}{dt} = \frac{2}{p \frac{2}{1-e^2}} n (4 + e^2 - 5 \sin^2 i + 5 (\sin^2 i - e^2) \cos 2!) \quad (42d)$$

$$\frac{d}{dt} = \frac{2}{p \frac{2}{1-e^2}} n (2 + e^2 (3 - 5 \cos 2!)) \cos i \quad (42e)$$

The above calculation was performed in the equatorial frame, without taking its precession into consideration. Had we taken into account the precession, we would get, on the right-hand side of (42) resonances between the motion of the Sun relative to the planet and the equinoctial precession. Since the time scale of the former exceeds, by orders of magnitude, the time scale of the latter, we may safely neglect these resonances. This justifies our neglect of the frame precession in the above calculation.

Finally, the calculation of the orbital elements' evolution is performed via Lagrange-type planetary equations, whose right-hand sides combine those of (1–5) and (42).

3 A purely numerical treatment of the problem

Our main goal is to check the applicability (both in terms of the initial conditions and the permissible time scales) of our approximate system (1–5) written for the osculating elements introduced in a frame co-precessing with the equator of date. This check will be performed by an independent straightforward, purely numerical, computation that will be free from whatever simplifying assumptions. The check will be carried out in terms of Cartesian coordinates and velocities defined in an inertial frame of reference. Both the semi-analytical calculation of the elements in a coprecessing frame and the straightforward numerical integration in inertial Cartesian axes will be carried out for Deimos.

3.1 The numerical algorithm, the units, the constants, and the initial conditions.

The numerical integration of Deimos' orbit can be performed using Cartesian coordinates in the J1950 inertial reference frame. As we also have to compute the Martian polar axis motion, there are two vector differential equations to integrate simultaneously. One is the Newton gravity law:

$$\ddot{\mathbf{r}} = \frac{G(M + m)\mathbf{r}}{r^3} + Gm^0 \frac{\mathbf{r}^0}{\mathbf{r}^0} \frac{\mathbf{r}^0}{\mathbf{r}^3} + G(M + m)\mathbf{r}\mathbf{U}; \quad (43)$$

where $\mathbf{r}\mathbf{U}$ has components

$$\begin{aligned} \mathbf{e}_x \mathbf{U} &= \frac{e^2 J_2}{r^4} \frac{x}{r} \frac{15}{2} \sin^2 \frac{3}{2} \sin \sin \mathbf{i}_p \sin h_p \\ \mathbf{e}_y \mathbf{U} &= \frac{e^2 J_2}{r^4} \frac{y}{r} \frac{15}{2} \sin^2 \frac{3}{2} + 3 \sin \sin \mathbf{i}_p \cosh h_p \\ \vdots \mathbf{e}_z \mathbf{U} &= \frac{e^2 J_2}{r^4} \frac{z}{r} \frac{15}{2} \sin^2 \frac{3}{2} \sin \cos \mathbf{i}_p : \end{aligned} \quad (44)$$

Here and $\mathbf{r} = (x; y; z)$ denote, correspondingly, the latitude of Deimos relative to the Martian equator and the position vector of Deimos related to the Martian center of mass; e is the Martian equatorial radius; M and m stand for the masses of Mars and Deimos, respectively. Angles h_p and \mathbf{i}_p are the longitude of the node and the inclination of the planet's equator of date relative to that of epoch. Without loss of generality, we identify the equator of epoch with the XY plane of the J1950 coordinate system. This enables us to assume that the above equation (44) is written down in this system. Integration in this, inertial, frame offers the obvious advantage of nullifying the inertial forces.

Table 1 gives the initial conditions for our simulation, expressed in terms of the Keplerian orbital elements. Table 2 presents these initial conditions in a more practical form, i.e., in terms of the Cartesian positions and velocities corresponding to the said elements. A transition from the Keplerian elements to these Cartesian positions and velocities is a two-step process. First, we take orbital elements defined in a frame associated with the Martian equator of date (i.e., in a frame coprecessing but not corotating with the planet) and transform them into Cartesian coordinates and velocities defined in that same frame. Then, by two successive rotations of angles \mathbf{i}_p and h_p , we transform them into Cartesian coordinates and velocities related to the J1950 reference frame. These initial positions and velocities were used to begin the integration.

At each step of integration of (43), the same two rotations are performed on the components $\mathbf{r}\mathbf{U}$ given by (44). As mentioned above, to avoid the absence of inertial forces on the right-hand side of (43) one must write down and integrate (43) in the inertial J1950 frame. Since the analytical expressions (44) for $\mathbf{r}\mathbf{U}$ contain the latitude \mathbf{r} , they are valid in the coprecessing coordinate system and, therefore, need to be transformed to J1950 at each step. To carry out the transformation, one needs to know, at each step, the relative orientation of the Martian polar axis and the inertial J1950 coordinate system. The orientation is given by the aforementioned Colombo model. This is how our second equation, the one of Colombo, comes into play:

$$\frac{d\mathbf{k}}{dt} = (\hat{\mathbf{k}} \times \hat{\mathbf{k}})(\hat{\mathbf{n}}) : \quad (45)$$

All in all, we have to integrate the system (43 – 45). Table 3 gives the initial conditions used for integrating (45), while Table 4 gives the numerical values used for the parameters involved.

The software used for numerical integration of the system (43 – 45) is called NOE (Numerical Orbit and Ephemerides), and is largely based on the ideas and methods developed in Lainey, Duriez & Vienne (2004). This numerical tool was created at the Royal Observatory of Belgium mainly for computations of the natural satellite ephemerides. It is an N-body code, which incorporates highly sensitive modelling and can generate partial derivatives. The latter are needed when one wants to fit the initial positions, velocities, and other parameters to the observation data. To save the computer time, an optimised force subroutine was built into the code, specifically for integrating the above equations. This appliance, based on the RA15 integrator offered by Everhart (1985), was chosen for its speed and accuracy. During the integration, a variable step size with an initial value of 0.04 day was used. To control the numerical error, back and forth integrations were performed. In particular, we carried out a trial simulation consisting of a thousand-year forward and a subsequent thousand-year back integration. The satellite displacement due to the error accumulated through this trial was constrained to 150 meters. Most of this 150 meter difference comes from a numerical drift of the longitude, while the numerical errors in the computation of the semi-major axis, the eccentricity, and the inclination were much lower. These errors were reduced for this trial simulation to only 10^5 km, 10^{10} , and 10^{10} degree, respectively. This provided us with a high confidence in our subsequent numerical results.

As a complement to the said back-and-forth check, the energy-conservation criterium was used to deduce, in the first approximation, an optimal initial step-size value and to figure out the numerical error proliferation. (It is for this energy-conservation test that we introduced a non-zero mass for Deimos. Its value was taken from Smith, Lemoine & Zuber (1995).) Applicability of this criterium is justified by the fact that the numerical errors are induced mostly by the fast orbital motion of the satellite.⁴

parameters	numerical values
a	23459 km
e	0.0005
i	0.5 deg. and 89 deg.
	10 deg.
!	5 deg.
M	0 deg.

Table 1: The orbital elements' values taken as initial conditions for our simulations.

⁴ Although the planet-satellite system is subject to an external influence (the solar torque acting on the planet), over short time scales this system can be assumed closed. In order to check the integrator's efficiency and to determine an optimal initial step size, we carried out auxiliary integrations of (43) – (44), with the Colombo equation (45) neglected and with the energy presumed to conserve. These several-thousand-year-long trial integrations, with the energy-conservation criterium applied, led us to the conclusion that our integrator remained steady over long time scales and that the initial step of 0.04 day was optimal. Then this initial step size was employed in our integration of the full system (43) – (45).

satellite	x	y	z
position km (i = 0.5)	23358.6525447458	2040.90967963532	-35.9715582515763
velocity km s ⁻¹ (i = 0.5)	-0.117066266533499	1.34018324055820	0.133068449913892
position km (i = 89)	22291.4778850948	6256.65104491350	-3706.42501342002
velocity km s ⁻¹ (i = 89)	0.231350273413379	3.619316279591354	1.33141651910815

Table 2: The initial positions and velocities used for D ein os, in the Earth equatorial J1950 frame centered on Mars. The first two rows correspond to the low-inclination case (0.5 degrees); the last two rows correspond to the high-inclination case (89 degrees).

parameters	numerical values
$I_p(t_0)$	5.156620156177409 deg.
$h_p(t_0)$	5 deg.

Table 3: Initial conditions used for the integration of equation (45).

parameters	numerical values
Martian mass (G M)	42830 km ³ s ⁻²
J_2	1960.45 10^6
Equatorial radius	3397 km
D ein os mass	0.091 10^3 km ³ s ⁻²
	3.9735 10^5 rad/yr

Table 4: Parameters' values used in our simulations.

3.2 The results of the straightforward integration.

The theory of satellite-orbit evolution, based on the planetary equations (1 – 5), is semi-analytical. This means that these equations for the elements' secular parts are derived analytically, but their integration is to be performed numerically. This integration was carried out using an 8th-order Runge-Kutta scheme with relative and absolute tolerances of 10^{-12} . Kilograms, years, and kilometers were taken as the mass, time, and length units, correspondingly.

3.2.1 Technicalities

To integrate the planetary equations (1 – 5), one should know, at each time step, the values of I_p and h_p , which are the time derivatives of the inclination and of the longitude of the node of the equator of date with respect to the equator of epoch. These derivatives will be rendered by the Colombo equation (17), after formulae (15 – 16) get inserted therein:

$$\begin{aligned} I_p = & q^2 \sin I_p \sin h_p \cosh h_p - qp \sin I_p + 2pq \sin I_p \cos^2 h_p \\ & p \sin I_p \cosh h_p \sin h_p + q \frac{p}{1 - q^2 - p^2} \cos I_p \cosh h_p \\ & p \frac{p}{1 - q^2 - p^2} \cos I_p \sin h_p ; \end{aligned} \quad (46)$$

and

$$\begin{aligned} h_p = & p - 2p \cos^2 I_p \cosh h_p + \frac{(-q + 2q \cos^2 I_p) \cos^2 h_p}{\sin h_p} \frac{2q \cos^2 I_p + q}{\sin I_p} \frac{p}{1 - p^2 - q^2} \\ & + q^2 p \cos I_p \cos^2 h_p + p^2 2q + 1 \cos I_p \\ & + \frac{2qp \cos I_p \cos^3 h_p}{\sin h_p} \frac{2pq \cosh h_p \cos I_p}{\sin h_p} ; \end{aligned} \quad (47)$$

Equations (46) and (47) are then integrated (with the initial conditions $I_p(t_0)$ and $h_p(t_0)$ borrowed from Table 3) simultaneously with the planetary equations (1 – 5). Through formulae (6), the above expressions for I_p and h_p yield the expressions for the components of $\dot{\omega}_1$. As can be seen from (12 – 14), integration of (1 – 5) also requires the knowledge of the derivatives $\dot{\omega}_1$, $\dot{\omega}_2$, and $\dot{\omega}_3$ at each integration step. These can be readily obtained by differentiating (6). The resulting closed-form expressions for $\dot{\omega}_1$, $\dot{\omega}_2$, and $\dot{\omega}_3$ are listed in Appendix A. The final step required for numerical integration of equations (1) – (5) is substitution of formulae (9 – 12), with the initial conditions from Table 1.

3.2.2 The plots and their interpretation

Fig. 1 depicts the history of the planetary equator, in the Colombo approximation, over 1 Bln years. The inclination exhibits long-periodic oscillations bounded within the range of 1.8 deg I_p – 12.3 deg, while the node regresses at a rate of $h_p = 0.00225$ deg=yr.

Integration of our semi-analytical model gives plots depicted in Figures 2 and 3, for a low initial inclination, and in Figures 4 and 5, for a high initial inclination. From Fig. 2 we see

that the variable equinoctial precession does not in fact considerably change the satellite's inclination on the precessing equator of date: the orbit inclination remains bounded within the region $0.495 \text{ deg} \leq i \leq 0.502 \text{ deg}$. This means that the "Goldreich lock" (inclination locking, predicted by the Goldreich (1965) model for small inclinations and for uniform equinoctial precession) works also for nonuniform Colombo precession of the equator. Similarly, the variations of the equinoctial precession exert virtually no influence upon the satellite node dynamics: it regresses at an almost constant rate of $-\tau_{\text{near equatorial}} = 6.435 \text{ deg/yr}$. The periapse precession rate remains virtually constant, as shown in Fig. 3. The semi-major axis and eccentricity vary only slightly. Both in the near-equatorial case (as in Fig. 3) and the near-polar case (as in Fig. 5), this behaviour of a and e confirms the analytical predictions given by formula (44) in Efron (2006), predictions that were derived from the appropriate planetary equations.

However, it must be emphasized that the inclusion of the precession into the model quantitatively modifies the behavior of the inclination. If only the oblateness and solar gravity effects were included in the model, then, at near-zero initial inclinations, one would expect the inclination to remain strictly locked, or "frozen" at its initial value. This is evident from Eq. (42c). The precession terms violate the frozen conditions and hence the inclination exhibits oscillations at the vicinity of its initial value. This is shown in Fig. 2, which depicts a comparison between the full model (oblateness, solar pull, precession) and a model where the precession is neglected. It is also evident from this figure that the nodal regression becomes slower when precession is neglected.

To continue, consider a hypothetical Martian satellite initially set on a near-polar orbit: $i_0 = 89 \text{ deg}$. Similarly to the near-equatorial case, the variations of the equinoctial precession make virtually no influence upon the node regression, as seen in Figure 4. The "Goldreich lock," too, stays intact: the inclination is bounded within the interval $88.75 \text{ deg} \leq i \leq 89.1 \text{ deg}$. Thus, even though the Goldreich (1965) calculations are not designed to work at high inclinations (see the subsection below), the main outcome, the inclination "locking," remains valid even for near-polar orbits. On the other hand, in the behaviour of i we can see an unusual pattern (the "crankshaft" features (Fig. 9)).

As in the near-equatorial case, the near-polar case is a good example for the influence of the precession on the orbital dynamics. Fig. 4 depicts the results of a simulation wherein the precession is completely neglected. In this case, the near-equatorial case, without the precession, provides a "frozen" orbit. This is evident from Eq. (42c). However, similarly to the near-equatorial case, the precession violates the frozen orbit conditions and an inclination excursion is observed.

The plots in Fig. 5 depict the time evolution of a , e , and i . The node steadily regresses at a rate of $-\tau_{\text{near polar}} = 0.121 \text{ deg/yr}$. The manifest difference between $-\tau_{\text{near equatorial}}$ and $-\tau_{\text{near polar}}$ is very easily understood simply from looking at the right-hand sides of equations (5) and (42). We see that, very roughly,

$$\begin{aligned}
 -\frac{3}{2}nJ_2 - \frac{e^2}{a} \frac{\cos i}{(1-e^2)^2} - \frac{n}{\sin i} \frac{p^2}{1-e^2} &= n^2 + e^2 (3 - 5 \cos 2i) \cos i \\
 \frac{3}{2}nJ_2 - \frac{e^2}{a} + 4n \cos i h_p \cos I_p &:
 \end{aligned} \tag{48}$$

Due to the smallness of n , the singular term with $\sin i$ in the denominator causes problems only within the narrowest vicinity of the equator. This singularity, however, is not physical, but is merely a matter of our choice of the elements. For near-polar orbits, this term plays a considerable role only in the closest vicinity (arc minutes) of $i = 90^\circ$, i.e., in the domain where

the term s proportional to $\cos i$ becomes very small. This means that orbits so close to the pole may demonstrate behaviour different from what we saw in Figure 4. This phenomenon will be studied below.

To examine the precision of our semi-analytical model implemented by equations (1–5) and (42), we have compared the results entailed by this model with those stemming from a purely numerical integration performed in terms of Cartesian coordinates and velocities (see subsection 3.1). The necessity for this check was dictated, mainly, by the fact that within the semi-analytical model the short-period terms are averaged out,⁵ while the straightforward numerical integration of (43–44) neglects nothing. We carried out the comparison of the two methods over 20 M yr only. The outcomes, both for $i_0 = 0.5$ degrees and $i_0 = 89$ deg, were in a good agreement with the afore discussed results furnished by our semi-analytical method. As an example, Fig. 6 shows the differences in inclination evolution in the case of $i_0 = 0.5$ deg (top figure) and $i_0 = 89$ deg (bottom figure) calculated by the semi-analytical and by the purely numerical methods over 20 M yr. The differences in inclinations are normalized by the initial inclination, and the results are depicted in percent. It is seen that there is a good match between the models; in the $i_0 = 0.5$ deg case the models match to within 1.3% while in the $i_0 = 89$ deg the models match to within 0.3%.

All in all, the outcome of our computations is two-fold. First, we have made sure that the semi-analytical model perfectly describes the dynamics over time scales of, at least, dozens of millions of years. Stated differently, the short-period terms and the terms of order 0 (\sim^2) play no role over these time spans. Second, we have made sure that the "Goldreich lock" initially derived for very low inclinations and for uniform equinoctial precession, works well also for variable precession and even for high inclinations, at least in the above example with $i_0 = 89$ deg.

3.2.3 Looking for trouble

A natural question arises as to whether the considered examples are representative. One may enquire if, perhaps, there still exists a combination of the initial conditions yielding noticeable variations of the satellite orbit inclination in the course of the primary's variable equinoctial precession over vast spans of time. To answer this question, we should scan through all the possible combinations of initial conditions, to identify a particular combination that would entail a maximum inclination excursion relative to the initial inclination. Stated more formally, we should seek a set of initial conditions $f h_{p_0}^?; I_{p_0}^?; i_0^?; \dot{i}_0^?; \dot{I}_0^?$ maximising the objective function $j_i(t) - i_0$:

$$f h_{p_0}^?; I_{p_0}^?; i_0^?; \quad ?_0^?; !_0^? g = \underset{\substack{t \in h_{p_0} \cap I_{p_0} \\ i_0; \quad o; \quad ;_0}}{\arg \max} f(t) \quad \quad \quad (49)$$

This problem belongs to the realm of optimisation theory. The optimisation space is constituted by the entire multitude of the permissible initial conditions. The sought after combination of initial conditions will be called the optimals set.

In this situation, the traditional optimisation schemes (such as the gradient search or the simplex method) may fail due to the rich dynamical structure of our problem: these methods may lead us to a local extremum. Thus, the search needs to be global. It can be carried out by means of Genetic Algorithms (GA's) [13, 15, 16, 17]. These are wont to supersede the traditional optimisation procedures in the following aspects. First, instead of directly dealing with the parameters, the GA's employ codings (usually, binary) of the parameter set ("strings," in the GA

⁵ Be mindful that in equations (1 – 5) the exact \sim -dependent terms are substituted with their orbital averages (12 – 14).

term inology). Second, instead of addressing a single point of the optimisation space, the GA's search from a population of the initial conditions. Third, instead of processing derivatives or whatever other auxiliary information, the GA's use only objective-function evaluations ("fitness evaluations"). Fourth, instead of deterministic rules to reiterate, the GA's rely upon probabilistic transition rules. Additional details on the particular GA mechanism used herein can be found in Appendix B.

A GA optimisation was implemented using the parameter values given in Table 5. The search

parameters	numerical values
Population size	30
Number of generations	100
String length	16bit
Probability of crossover	0.99
Probability of mutation	0.02

Table 5: Parameter values used for the GA optimisation

for the inclination-maximising initial conditions resulted in the following set:

$$I_{p0}^? = 4.847 \text{ deg}; h_{p0}^? = 202.529 \text{ deg}; i_0^? = 90.579 \text{ deg}; \Omega_0^? = 129.334 \text{ deg}; \omega_0^? = 284.783 \text{ deg} : (50)$$

Thus, the initial orbit is retrograde and, not surprisingly, very-near-polar. (See the discussion after formula (48).) The resulting time histories for a 1 Byr integration are depicted in Fig. 7, for i and Ω . In both cases the inclination amplitude is relatively large, $\max_{t \in [0, 10^9]} |i(t) - i_0| \approx 1 \text{ deg}$, but qualitatively, it still complies with inclination locking.

This example clearly shows that the precession is an important effect. As shown in the upper pane of Fig. 7, had we neglected the precession, a "frozen" inclination would have been obtained. This is expected, due to the fact that the solar pull guarantees frozen orbits at near-polar inclinations (cf. Eq. (42c)). However, the inclusion of the precession in the model qualitatively modifies the behavior, inducing large-magnitude chaotic variations of the inclination. This effect cannot be detected without including the precession alongside the oblateness and solar gravity.

Finally, here again, a comparison of the semi-analytical theory with the pure numerical integration was carried out, and it completely confirmed this weak chaotic behaviour.

4 Comparison of the numerical calculations and Goldreich's model

The next step in our study will be to compare the semi-analytical model to Goldreich's approximation (22–26). To that end, we simulate our semi-analytical model, using the initial conditions (50), for a 20 Myr time scale and compare the outcome with that resulting from Goldreich's approximation simulated with the same initial conditions. The results of this comparison are depicted in Figs. 8–9. Specifically, Fig. 8 compares the time histories of I_p and h_p . The evolution of the equator's node h_p is virtually the same in both models, but there are noticeable differences in the dynamics of I_p . While Goldreich's approximation assumes a constant I_p , the semi-analytical model is based on the Colombo calculation of the equinoctial precession, calculation that predicts considerable oscillations within the range $1.36 \text{ deg} \leq I_p \leq 14.86 \text{ deg}$. This entails the difference between the dynamics predicted by our semi-analytical model and the dynamics stemming from

the Goldreich approximation. These differences, for i and \dot{i} , are depicted in Fig. 9. In Goldreich's model, i stays extremely close to the initial value, 90.39 deg ± 90.74 deg, which is the essence of the Goldreich lock. However, in the more accurate, semi-analytical model we have 88.98 deg ± 91 deg. The time history of \dot{i} , too, reveals that Goldreich's approximation does not adequately model the actual dynamics, since it predicts a much larger secular change than the semi-analytical model.

All in all, the dynamics (i.e., particular trajectories) predicted by the two models are quantitatively different. At the same time, when it comes to the most physically important conclusion from the Goldreich approximation, the "Goldreich lock," one may still say that, qualitatively, the semi-analytical model confirms its existence even for variable equinoctial precession, and even for highly inclined satellite orbits. It is, though, not as strict as predicted by the Goldreich model: we can see from Fig. 9 that the orbit inclination varies within a two-degree span, while the Goldreich approximation would constrain it to small shares of a degree.

An intriguing new feature of the inclination evolution, which manifests itself for orbits close to polar, is the "crankshaft" feature. This kind of behaviour, well depicted in Fig. 9, is not rendered by the Goldreich model, because that model was initially developed for small inclinations. One might suspect that the "crankshaft" is merely a numerical artefact, had it not been discovered under different circumstances (in the absence of precession but in the presence of a third body) by Zhang & Hamilton (2005). This kind of pattern may be generic for the close vicinity of $i = 90$ deg. In our case, the approximate formula (48) drops us a hint that the dynamics may become unexpected on a very close approach to $i = 90$ deg, when the second term becomes dominant in the right-hand side of (48). Whether the "crankshaft" feature is a physical effect in its own right, should be examined by means of a more comprehensive model that includes the tides. This work will be done in Lainey, Efron, & Gurli (2007).

5 Conclusions

In the article thus far, we continued developing a tool for exploring long-term evolution of a satellite orbit about a precessing oblate primary. In particular, we were interested in the time-dependence of the orbit inclination relative to the moving equator of date. Our model includes three factors: the J_2 of the planet, its nonuniform equinoctial precession described by the Colombo formalism, and the gravitational pull of the Sun. The problem was approached using different methods. One, semi-analytical, was based on numerical integration of simplified and averaged Lagrange-type equations for the secular parts of the Keplerian orbitalelements introduced in a noninertial reference frame coprecessing with the planetary equator of date. The right-hand sides of these five equations consisted of the precession-generated contributions (1–5) borrowed from Efron (2006), and the contributions (42) due to the direct pull of the Sun. The other approach was a straightforward, purely numerical, computation of the satellite dynamics using Cartesian coordinates in the J1950 inertial reference frame.

The results of both computations have demonstrated a good agreement over 20 M yr. This means that the semi-analytical model adequately describes the dynamics over time spans of, at least, dozens of millions of years. Specifically, the terms neglected in the semi-analytical model (the short-period terms and the terms of order $O(\sim^2)$) play no significant role on these time scales.

Our calculations have shown the advantages and the limitations of the simple model developed by Goldreich (1965) for uniform equinoctial precession and low inclinations. Though his model does not adequately describe the dynamics (that turns out to be weakly chaotic), them are physical

prediction of Goldreich's model { the "Goldreich lock" { sustains the variations of equinoctial precession. To some extent, this prediction remains valid even at large inclinations: variations of the satellite orbit inclination on the precessing equator of date always remain small { dozens of arcseconds, for low-inclination orbits, and about two angular degrees, for high-inclination orbits.

A subtle feature in the inclination dynamics, feature that is not accounted for by the Goldreich model, is the "crankshaft" that shows itself for near-polar orbits (Fig. 7 and Fig. 9). To safely claim that this feature is physical, we shall have to check it with the tidal forces brought into consideration. (Lainey, E from sky & Gur 12007)

Finally, we carried out a comparison of the general model to a model wherein the equinoctial precession is neglected. It was shown that the frozen orbits (both near-equatorial and near-polar), obtained with only the oblateness and solar pull taken into account, disappear when the equinoctial precession is included in the model. Instead, chaotic variations of the inclination emerge.

Appendix A : Closed-Form Expressions for $\omega_1; \omega_2; \omega_3$

Using the compact notation $c_{(1)} = \cos(\omega)$ and $s_{(1)} = \sin(\omega)$, and conforming to the procedure described in the text, we obtain the following expressions for $\omega_1; \omega_2; \omega_3$:

$$\begin{aligned}
\omega_1 &= (((6p^2q^2 - p^4 - q^4)(c_{I_p})^3 + (-6p^2q^2 + p^4 + q^4)c_{I_p})(a_{h_p})^4 \\
&+ ((3p^4 - 6p^2q^2 - 3q^2 + 3p^2 + 5q^4)(c_{I_p})^3 + (2p^4 - 4q^4 + 6p^2q^2 - 2p^2 + 2q^2)c_{I_p}) \\
&\quad (c_{h_p})^2 + (3q^2 - 3p^2q^2 - 4q^4)(c_{I_p})^3 + (3q^4 - 2q^2 + 2p^2q^2)c_{I_p} \\
&+ ((4qp^3 - 4q^3p)(c_{I_p})^3 + (4q^3p - 4qp^3)c_{I_p})(a_{h_p})^5 + (2qp^3 - 6qp + 14q^3p)(c_{I_p})^3 \\
&+ ((12q^3p + 4qp)(c_{I_p})^3 + ((6qp - 10q^3p - 6qp^3)(c_{I_p})^3 + (4qp^3 + 8q^3p - 4qp)a_{h_p}) \\
&\quad (s_{h_p})^1 (s_{I_p})^1 + (((9pq^2 + 9pq^4 - 3p^5 + 3p^3 + 6p^3q^2)(c_{I_p})^2 + 3pq^2 - 2p^3q^2 + p^5 \\
&\quad 3pq^4 - p^3)(c_{h_p}^3) + ((11p^3q^2 - p^5 - 10pq^4 - p + 2p^3 + 11pq^2)(c_{I_p})^2 + 3pq^4 + 3p^3q^2 \\
&\quad 3pq^2)a_{h_p} + (((9p^2q + 6p^2q^3 + 9p^4q - 3q^5 + 3q^3)(c_{I_p})^2 - 3p^4q + 3p^2q - 2p^2q^3 \\
&\quad q^3 + q^5)(c_{h_p}^4) + ((7p^2q - p^2q^3 - 8q^3 - 8p^4q + 7q^5 + q)(c_{I_p})^2 - 2q^5 + p^2q^3 + 2q^3 \\
&+ 3p^4q - 3p^2q)(c_{h_p})^2 + (5q^3 - 4q^5 - q - 5pq^3 - p^4q + 2p^2q)(c_{I_p})^2 - q^3 + q^5 + p^2q^3) \\
&\quad (s_{h_p})^1 (s_{I_p})^1 \frac{1 - p^2 - q^2}{1 - p^2 - q^2})^2 (((2qp - 2qp^2)(c_{I_p})^2 + 2qp + 2qp)(a_{h_p})^2 \\
&+ (qp + qp)(c_{I_p})^2 - qp - qp + (((2pp + 2qq)(c_{I_p})^2 + 2pp - 2qq)(c_{I_p})^3 + ((2pp - 2qq)(c_{I_p})^2 \\
&\quad 2pp + 2qq)(c_{I_p})(s_{h_p})^1 (s_{I_p})^1 + ((qp^2 - 2q^2q + q - qp)(c_{I_p})^2 a_{h_p} \\
&+ \frac{(p - 2p^2p - pqq - p^2q)c_{I_p}(a_{h_p})^2 + (p + pq^2 + 2p^2p + pqq)c_{I_p})}{s_{h_p}} \frac{h_p}{1 - p^2 - q^2})^1) ; \quad (51)
\end{aligned}$$

$$\begin{aligned}
-2 &= (((4q^3p - 4qp^3)(c_{I_p})^2 + 4qp^3 - 4q^3p)(c_{h_p})^4 \\
&+ ((qp^3 - 7q^3p + 2qp)(c_{I_p})^2 - 3qp^3 + 5q^3p)(c_{h_p})^2 + (2q^3p - qp + qp^3)(c_{I_p})^2 \\
&\quad q^3p + (((6p^2q^2 - p^4 - q^4)(c_{I_p})^2 - 6p^2q^2 + p^4 + q^4)(c_{h_p}^5 + (3q^4 - q^2 - 9p^2q^2 + p^2)(c_{I_p})^2 \\
&\quad p^4 - 2q^4 + 9p^2q^2)(c_{h_p})^3 + ((p^2 + q^2 - 2q^4 + p^4 + 3p^2q^2)(c(I_p))^2 + q^4 \\
&\quad 3p^2q^2)c(h_p))(s_{h_p})^1)(s(I_p))^1 + ((-4p^2q^3 + 6p^2q - 2q^3 + 2q^5 - 6p^4q)c(I_p)(c_{h_p})^3 \\
&+ (2q^3 + 4p^4q + 2p^2q^3 - 4p^2q - 2q^5)c_{I_p}c_{h_p} + ((-2p^5 - 6p^2q + 6pq^4 + 4p^3q^2 + 2p^3)c_{I_p}(c_{h_p})^4 \\
&+ (2p^5 + 8pq^2 - 8p^4q - 6p^3q^2 - 2p^3)c_{I_p}(c_{h_p})^2 + (2pq^4 - 2p^2q + 2p^3q^2)c_{I_p})(s_{h_p})^1) \\
&\quad h_p \frac{1}{1 - p^2 - q^2} i_1^1)^2 - (((2pp - 2qq)(c_p)^3 + (-2pp + 2qq)c_p)(c_{h_p}^2 \\
&+ (2pp + 4qq)(c_{I_p})^3 + (-2pp - 4qq)c_p + (((-2qp - 2qp)(c_p)^3 + (2qp + 2qp)c_{I_p})(c_{h_p})^3 \\
&+ ((2qp + 2qp)(c(I_p))^3 + (-2qp - 2qp)c_p)c(h_p))(s_{h_p})^1)(s_{I_p})^1 \\
&+ ((-2pq^2 + 2pqq + 4p^2p - 2p)(c_p)^2 + p - 2p^2p - pqq - p^2q)c_{h_p} \\
&+ (((-2qpp - 2qp^2 - 4q^2q + 2q)(c_{I_p})^2 - q + qp^2 + 2q^2q + qpp)(c_{h_p}^2 \\
&+ (2qpp - 2q + 2qp^2 + 4q^2q)(c_{I_p})^2 - qp^2 - 2q^2q + q - qpp)(s(h_p))^1) h_p \frac{1}{1 - p^2 - q^2} i_1^1) ;
\end{aligned}$$

(52)

and

$$\begin{aligned}
\rightarrow &= (((4q^3p - 4qp^3)(c_{I_p})^2 + 4qp^3 - 4q^3p)(c_{h_p})^4 + ((qp^3 - 7q^3p + 2qp)(c(I_p))^2 \\
&\quad 3qp^3 + 5q^3p)(c_{h_p})^2 + (2q^3p - qp + qp^3)(c_{I_p})^2 - q^3p + (((6p^2q^2 - p^4 - q^4)(c_{I_p})^2 - 6p^2q^2 + p^4 \\
&\quad + q^4)(c(h_p))^5 + ((3q^4 - q^2 - 9p^2q^2 + p^2)(c_{I_p})^2 - p^4 - 2q^4 + 9p^2q^2)(c_{h_p})^3 + ((p^2 + q^2 - 2q^4 \\
&\quad + p^4 + 3p^2q^2)(c(I_p))^2 + q^4 - 3p^2q^2)c(h_p)(s_{h_p})^1)(s(I_p))^1 + ((-4p^2q^3 + 6p^2q - 2q^5 \\
&\quad 6p^4q)c(I_p)(c_{h_p})^3 + (2q^3 + 4p^4q + 2p^2q^3 - 4p^2q - 2q^5)c_{I_p}c_{h_p} \\
&\quad + ((-2p^5 - 6pq^2 + 6pq^4 + 4p^3q^2 + 2p^3)c_{I_p}(c_{h_p})^4 + (2p^5 + 8pq^2 - 8pq^4 - 6p^3q^2 - 2p^3)c_{I_p}(c_{h_p})^2 \\
&\quad + (2pq^4 - 2pq^2 + 2p^3q^2)c_{I_p}(s_{h_p})^1) \frac{p}{1 - p^3 - q^2})^2 (((2pp - 2qq)(\xi_p))^3 \\
&\quad + (-2pp + 2qq)c(I_p)(c(h_p))^2 + (2pp + 4qq)(c_{I_p})^3 + (-2pp - 4qq)\xi_p \\
&\quad + (((-2qp - 2qp)(\xi_p))^3 + (2qp + 2qp)c_{I_p}(c_{h_p})^3 + ((2qp + 2qp)(c(I_p))^3 \\
&\quad + (-2qp - 2qp)\xi_p)c(h_p)(s_{h_p})^1) (s_{I_p})^1 + (((2pq^2 + 2pqq + 4p^2p - 2p)(\xi_p))^2 + p \\
&\quad 2p^2p - pqq - p^2q)c_{h_p} + (((-2qpp - 2qp^2 - 4q^2q + 2q)(c(I_p))^2 - q + qp^2 + 2q^2q \\
&\quad + qpq)(c_{h_p})^2 + (2qpp - 2q + 2qp^2 + 4q^2q)(c_{I_p})^2 - qp^2 - 2q^2q + q - qpq)(s_{h_p})^1) \\
&\quad h_p \frac{i_1}{1 - p^3 - q^2}
\end{aligned} \tag{53}$$

Appendix B : Niching Genetic Algorithms

The most commonly used Genetic Algorithm (GA) is the so-called "Simple GA." To perform an evolutionary search, the Simple GA uses the operators of crossover, reproduction, and mutation. A crossover is used to create new solution strings ("children" or "offspring") from the existing strings ("parents"). Reproduction copies individual strings according to the objective function values. Mutation is an occasional random alteration of the value of a string position, used to promote diversity of solutions.

Although Simple GA's are capable of detecting the global optimum, they suffer from two main drawbacks. First, convergence to a local optimum is possible due to the effect of premature convergence, where all individuals in a population become nearly identical before the optimum has been located. Second, convergence to a single optimum does not reveal other optima, which may exhibit attractive features. To overcome these problems, modifications of Simple GA's were considered. These modifications are called niching methods, and are aimed at promoting a diversity of solutions for multimodal optimisation problems. In other words, instead of converging to a single (possibly local) optimum, niching allows for a number of optimal solutions to co-exist, and it lets the designer choose the appropriate one. The niching method used throughout this study is that of Deterministic Crowding. According to this method, individuals are first randomly grouped into parent pairs. Each pair generates two children by application of the standard genetic operators. Every child then competes against one of his parents. The winner of the competition moves on to the next generation. By using the notation P_i for a parent, C_i for a child, $f(\cdot)$ for a fitness, and $d(\cdot)$ for a distance, a pseudo-code for the two possible parent-child tournaments can be written as follows:

```

If  $d(P_1; C_1) + d(P_2; C_2) = d(P_1; C_2) + d(P_2; C_1)$ 
If  $f(C_1) < f(P_1)$  replace  $P_1$  with  $C_1$ 
If  $f(C_2) < f(P_2)$  replace  $P_2$  with  $C_2$ 

```

Else

If $f(C_1) < f(P_2)$ replace P_2 with C_1
If $f(C_2) < f(P_1)$ replace P_1 with C_2

In addition to applying the Deterministic Crowding niching method, we used a two-point crossover instead of a single-point one. In the Simple GA, the crossover operator breaks the binary string of parameters, the "chromosome," at a random point and exchanges the two pieces to create a new "chromosome." In a two-point crossover, the "chromosome" is represented with a ring. The string between the two crossover points is then exchanged. The two-point crossover or other multiple-point crossover schemes have preferable properties when optimisation highly nonlinear functions is performed.

Acknowledgments

ME is grateful to George Kaplan for numerous fruitful discussions on the subject, and to Marc Mardison for a consultation on the possible scenario of the Martian satellites capture. The work of ME was supported by NASA grant W-19948. The work of VL was supported by the European Community's Improving Human Potential Program under contract RTN 2-2001-00414 MAGE.

References

- [1] Brouwer, D. 1959. "Solution of the problem of artificial satellite theory without drag." The Astronomical Journal, Vol. 64, pp. 378 - 397.
- [2] Brumberg, V. A., Evdokimova, L. S.; & Kochina N. G. 1971. "Analytical Methods for the Orbits of Artificial Satellites of the Moon." Celestial Mechanics, Vol. 3, pp. 197 - 221.
- [3] Colombo, G. 1966. "Cassini's second and third laws." The Astronomical Journal, Vol. 71 pp. 891 - 896.
- [4] Efroimsky, M. Michael. 2002a. "Equations for the orbital elements. Hidden symmetry." Preprint No 1844 of the Institute of Mathematics and its Applications, University of Minnesota <http://www.ima.umn.edu/preprints/feb02/feb02.htm>
- [5] Efroimsky, M. Michael. 2002b. "The Implicit Gauge Symmetry Emerging in the N-body Problem of Celestial Mechanics." astro-ph/0212245
- [6] Efroimsky, M.; & Goldreich, P. 2003. "Gauge Symmetry of the N-body Problem in the Hamilton-Jacobi Approach." Journal of Mathematical Physics, Vol. 44, pp. 5958 - 5977 astro-ph/0305344
- [7] Efroimsky, M., & P. Goldreich. 2004. "Gauge Freedom in the N-body Problem of Celestial Mechanics." Astronomy & Astrophysics, Vol. 415, pp. 1187 - 1199 astro-ph/0307130
- [8] Efroimsky, M. 2004a. "On the theory of canonical perturbations and its application to Earth rotation. A source of inaccuracy in the calculation of angular velocity." Talk at the conference

\Journees 2004: Systèmes de référence spatio-temporels," l'Observatoire de Paris, 20 – 22 September 2004. astro-ph/0409282

[9] E from sky, M . 2004b. "Long-term evolution of orbits about a precessing oblate planet. 1. The case of uniform precession." astro-ph/0408168

This preprint is a very extended version of E from sky (2005). It contains a lengthy Appendix where all the necessary analytical calculations are explained in every detail.

[10] E from sky, M . 2005. "Long-term evolution of orbits about a precessing oblate planet: 1. The case of uniform precession." Celestial Mechanics and Dynamical Astronomy, Vol. 91, pp. 75 – 108.

[11] E from sky, M . 2006. "Long-term evolution of orbits about a precessing oblate planet: 2. The case of variable precession." To be published in Celestial Mechanics & Dynamical Astronomy. astro-ph/0607522

[12] Everhart, E . 1985. "An efficient integrator that uses Gauss-Radau spacings." Dynamics of Comets: Their Origin and Evolution. Proceedings of IAU Colloquium 83 held in Rome on 11 – 15 June 1984. Edited by A . Canisi and G . B . Valsecchi. Dordrecht: Reidel, Astrophysics and Space Science Library. Vol. 115, p. 185 (1985)

[13] Goldberg, D . E ., Genetic Algorithms in Search, Optimization and Machine Learning, Addison-Wesley, Reading, MA , 1989.

[14] Goldreich, P . 1965. "Inclination of satellite orbits about an oblate precessing planet." The Astronomical Journal, Vol. 70, p. 5 – 9

[15] Gur l, P ., Kasdin, N . J., Arnett, R . J., Seager S ., & Nissimke, S . 2002. "Infrared Space Observatories: How to Mitigate Zodiacal Dust Interference." The Astrophysical Journal, Vol. 567, pp. 1250 – 1261.

[16] Gur l, P ., & Kasdin, N . J. 2002. "Characterization and Design of Out-of-Ecliptic Trajectories Using Deterministic Crossing Genetic Algorithms." Computer Methods in Applied Mechanics and Engineering, Vol. 191, pp. 2169 – 2186.

[17] Gur l, P ., & Kasdin, N . J. 2002. "Nicheing Genetic Algorithms-Based Characterization of Geocentric Orbits in the 3D Elliptic Restricted Three-Body Problem ." Computer Methods in Applied Mechanics and Engineering, Vol. 191, pp. 5673 – 5696.

[18] Kinoshita, H . 1977. "Theory of the Rotation of the Rigid Earth." Celestial Mechanics, Vol. 15, pp. 277 – 326.

[19] Kozai, Y . 1960. "Effect of precession and nutation on the orbital elements of a close earth satellite." The Astronomical Journal, Vol. 65, pp. 621 – 623.

[20] Lainey, V ., Duriez, L . & Vienne, A . 2004. "New accurate ephemerides for the Galilean satellites of Jupiter. I. Numerical integration of elaborated equations of motion." Astronomy & Astrophysics, Vol. 420, pp. 1171 – 1183.

[21] Lainey, V ., E from sky, M ., & Gur l, P . 2007. "Long-term evolution of orbits about a precessing oblate planet: 4. A comprehensive model." In preparation.

[22] Lambeck, K ., 1980. *The Earth's Variable Rotation: Geophysical Causes and Consequences*. Cambridge University Press, London 1980.

[23] Laskar, J. 1988. "Secular evolution of the solar system over 10 million years." *Astronomy & Astrophysics*, Vol. 198, pp. 341 – 362.

[24] Laskar, J., & J. Robutel. 1993. "The Chaotic Oblliquity of the Planets." *Nature*, Vol. 361, pp. 608 – 612.

[25] Murray, M . 1988. "Satellite Capture and the Restricted Three-Body Problem ." *Ph.D. Thesis*, University of Wisconsin, Madison 1988.

[26] Newman, W ., & M . From sky. 2003. "The Method of Variation of Constants and Multiple Time Scales in Orbital Mechanics." *Chaos*, Vol. 13, pp. 476 – 485.

[27] Pang, K .D ., J.B .Pollack, J. Veverka, A .L .Lane, & J.M .A jello. 1978. "The Composition of Phobos: Evidence for Carbonaceous Chondrite Surface from Spectral Analysis." *Science*, Vol. 199, p. 64

[28] Pollack, J.B ., Burns, J.A ., & Tauber, M .E . 1979. "Gas Drag in Primordial Circumplanetary Envelopes. A Mechanism for Satellite Capture." *Icarus*, Vol. 37, p. 587

[29] Proskurin, V .F ., & B atrakov, Y .V . 1960. "Perturbations of the Motion of Artificial Satellites, caused by the Earth Oblateness." *The Bulletin of the Institute of Theoretical Astronomy*, Vol. 7, pp. 537 – 548.

[30] Smith, D .E .; Lemoine, F .G .; Zuber, M .T . 1995. "Simultaneous estimation of the masses of Mars, Phobos, and Deimos using spacecraft distant encounters," *Geophysical Research Letters*, Vol. 22, pp. 2171 – 2174.

[31] Szebehely, V . 1967. *Theory of Orbits*. Academic Press, NY .

[32] Tolson, R .H ., and 15 collaborators. 1978. "Viking First Encounter of Phobos. Preliminary Results." *Science*, Vol. 199, p. 61

[33] Touma, J., & J.W .Isdom . 1994. "Lie-Poisson Integrators for Rigid Body Dynamics in the Solar System ." *The Astronomical Journal*, Vol. 107, pp. 1189 – 1202.

[34] Veverka, J. 1977. "Phobos and Deimos." *Scientific American*, Vol. 236, p. 30

[35] Ward, W . 1973. "Large-scale Variations in the Oblliquity of Mars." *Science*. Vol. 181, pp. 260 – 262.

[36] Ward, W . 1974. "Climatic Variations of Mars. A astronomical Theory of Insolation." *Journal of Geophys. Research*, Vol. 79, pp. 3375 – 3386.

[37] Ward, W . 1979. "Present Oblliquity Oscillations of Mars – Fourth-order Accuracy in Orbital e and i." *Journal of Geophys. Research*, Vol. 84, pp. 237 – 241.

[38] Ward, W . 1982. "Comments on the long-term Stability of the Earth's Oblliquity." *Icarus*, Vol. 50, pp. 444 – 448.

[39] Zhang, K ., & Hamilton, D .P . 2005. "Dynamics of Inner Neptunian Satellites." *Abstracts of the 37th DPS Meeting of the American Astronomical Society*. In: *AAS Bulletin*, Vol. 37, pp. 667 – 668

Figures

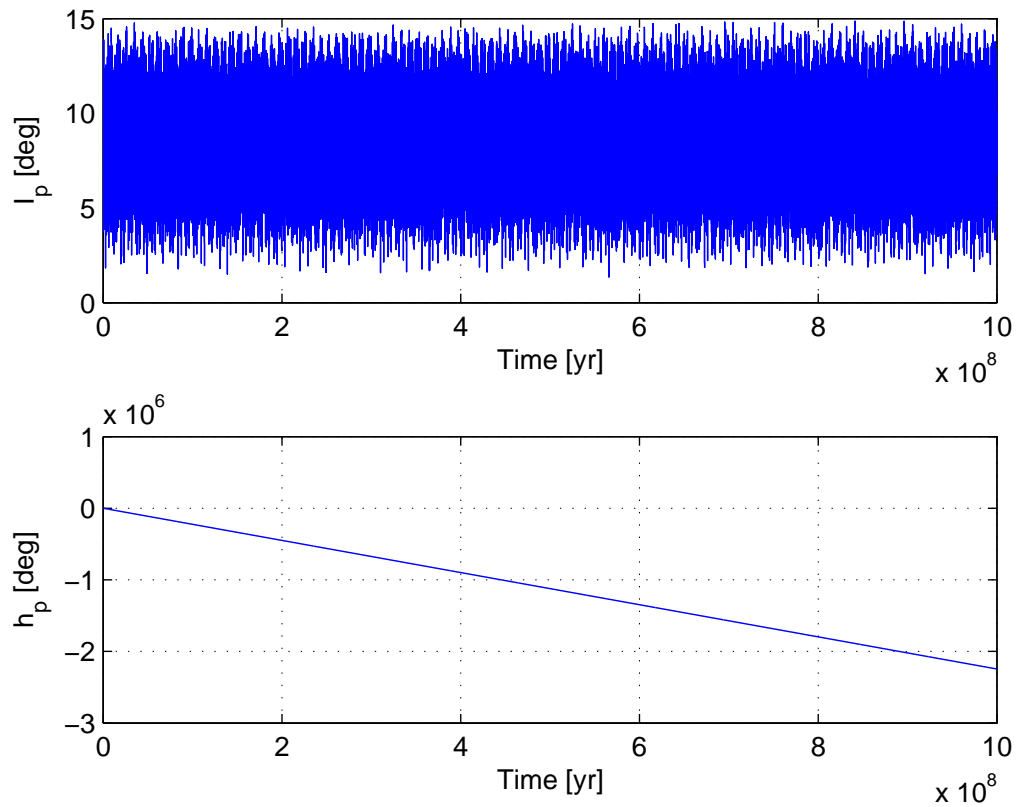


Figure 1: Evolution of the inclination and of the longitude of the node of the Martian equator of date relative to the equator of epoch, over 1 Byr, in the Colombo approximation.

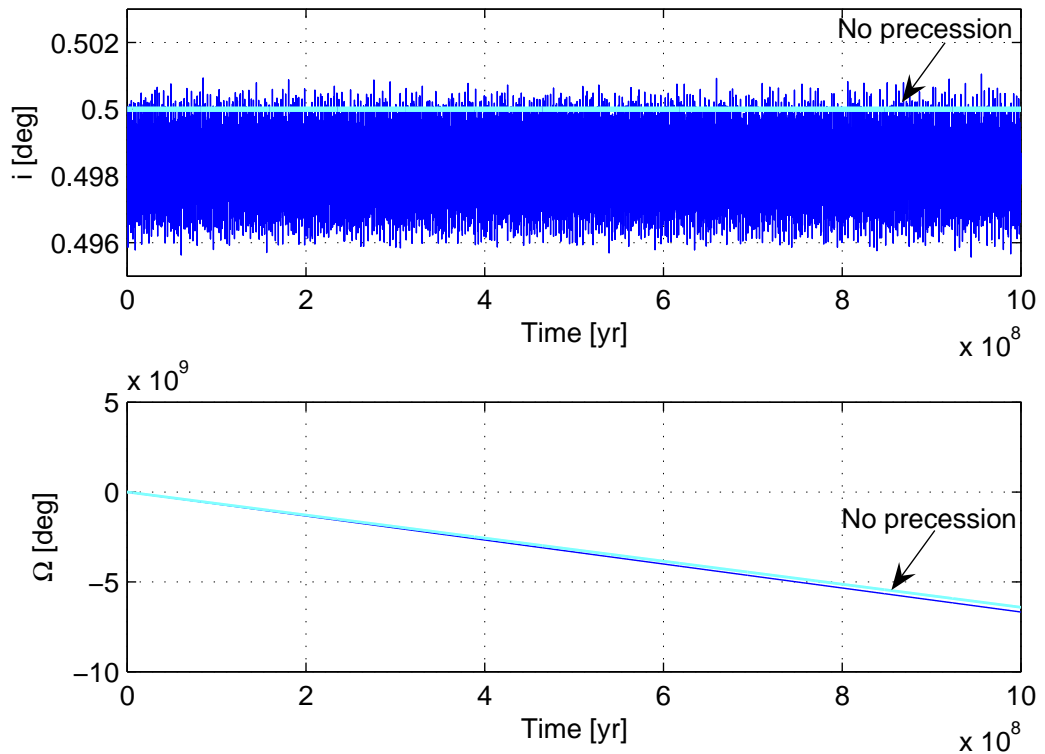


Figure 2: Evolution of the inclination (initially set to 0.5 degree) and of the longitude of the node of Démis over 1 Gyr. The plot, obtained by integration of the semi-analytical model, exhibits inclination locking and a uniform regression of the node; when precession is neglected, the inclination remains frozen at its initial value.

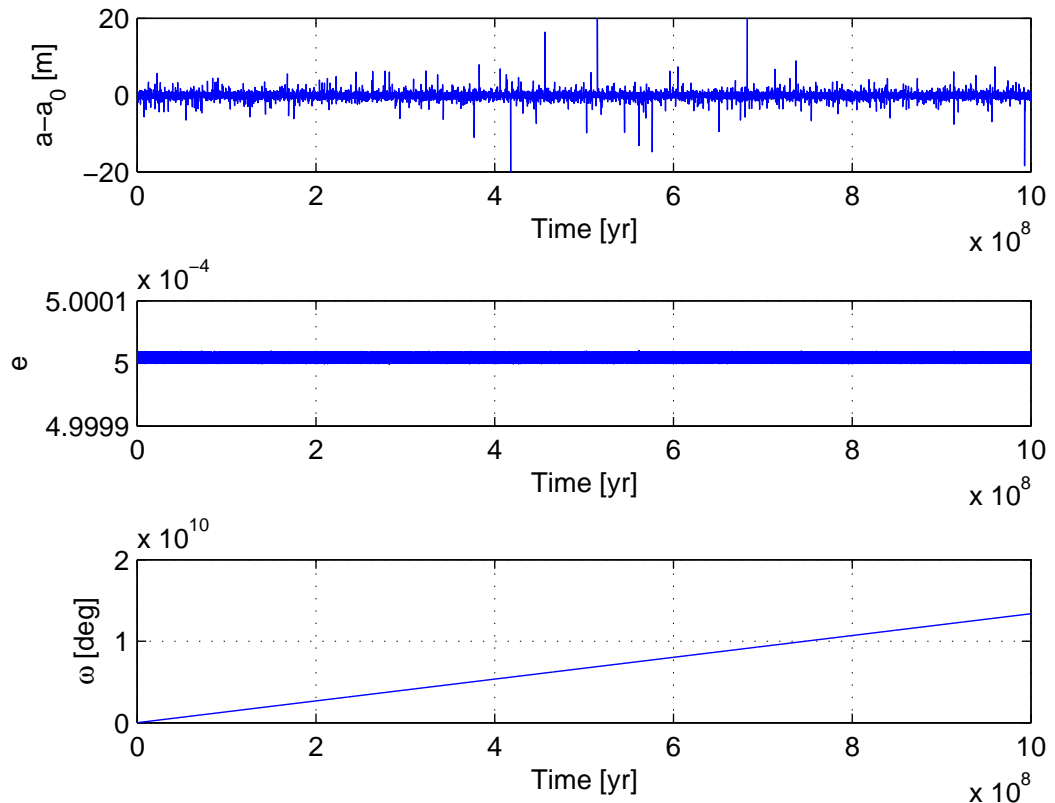


Figure 3: Evolution of the semi-major axis, eccentricity, and argument of periapsis of Daimos over 1 B yr. (The inclination was initially set to 0.5 degree.) Both the semi-major axis and eccentricity exhibit quasiperiodic motion about their initial values. (The variations of the semi-major axis are so small that it is more convenient to plot $a - a_0$ rather than a .) The plots were obtained by integration of the semi-analytical model.

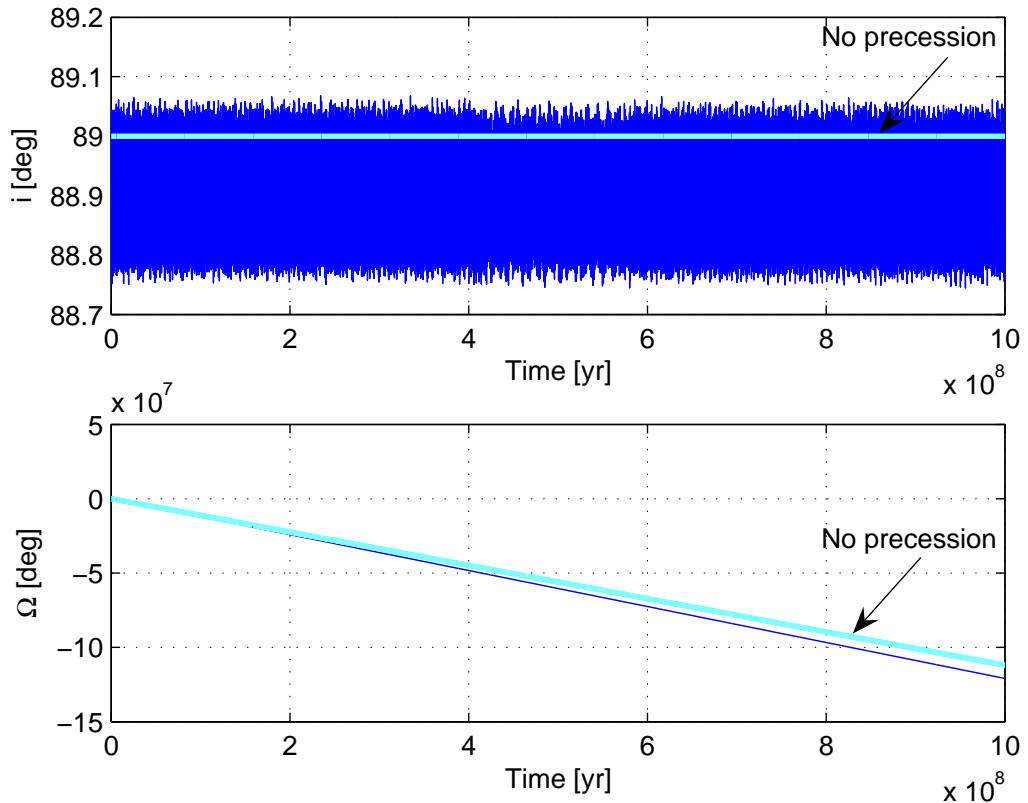


Figure 4: Evolution of the inclination and of the longitude of the node of Daimos over 1 B yr. (The inclination was initially set to 89 degrees.) The plot, obtained by integration of the semi-analytical model, exhibits inclination locking and a uniform regression of the node; if precession is neglected, the inclination remains frozen at its initial value, and the regression of the nodes is slower.

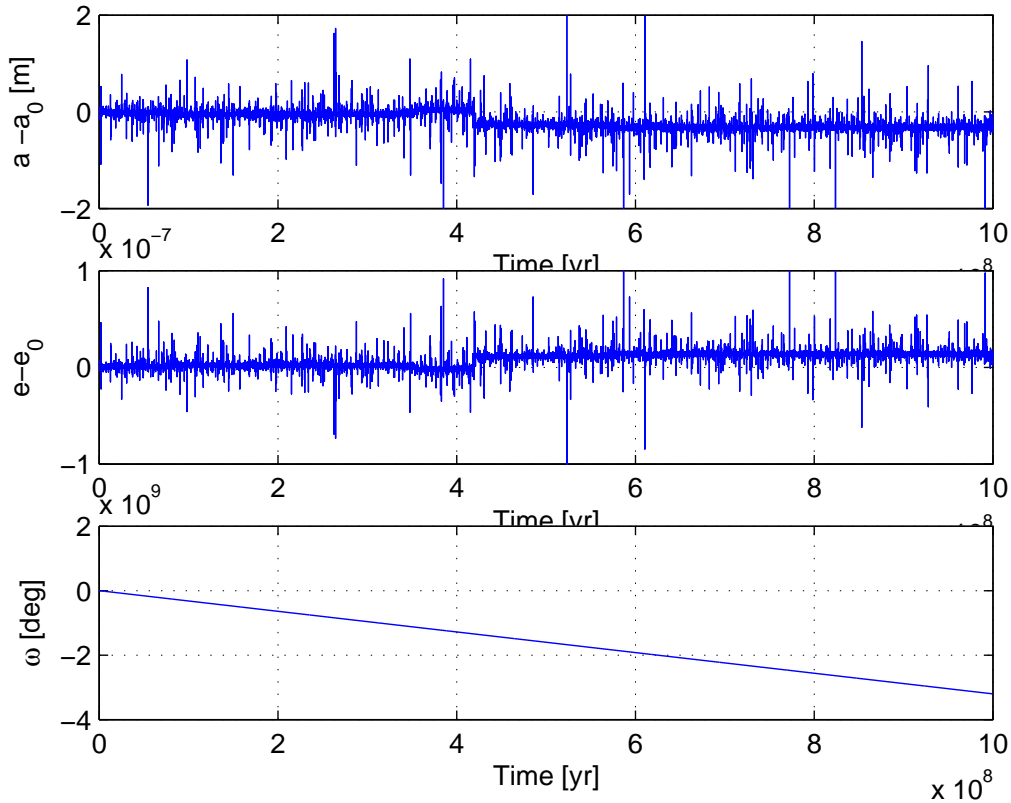


Figure 5: Evolution of the semi-major axis, eccentricity, and argument of periapsis of Daimos over 1 Gyr. (The inclination was initially set to 89 degrees.) The semi-major axis and eccentricity exhibit long-periodic motion about the initial value. (The variations of the semi-major axis are so small that it is more convenient to plot $a - a_0$ rather than a .) The plots were obtained by integration of the semi-analytical model.

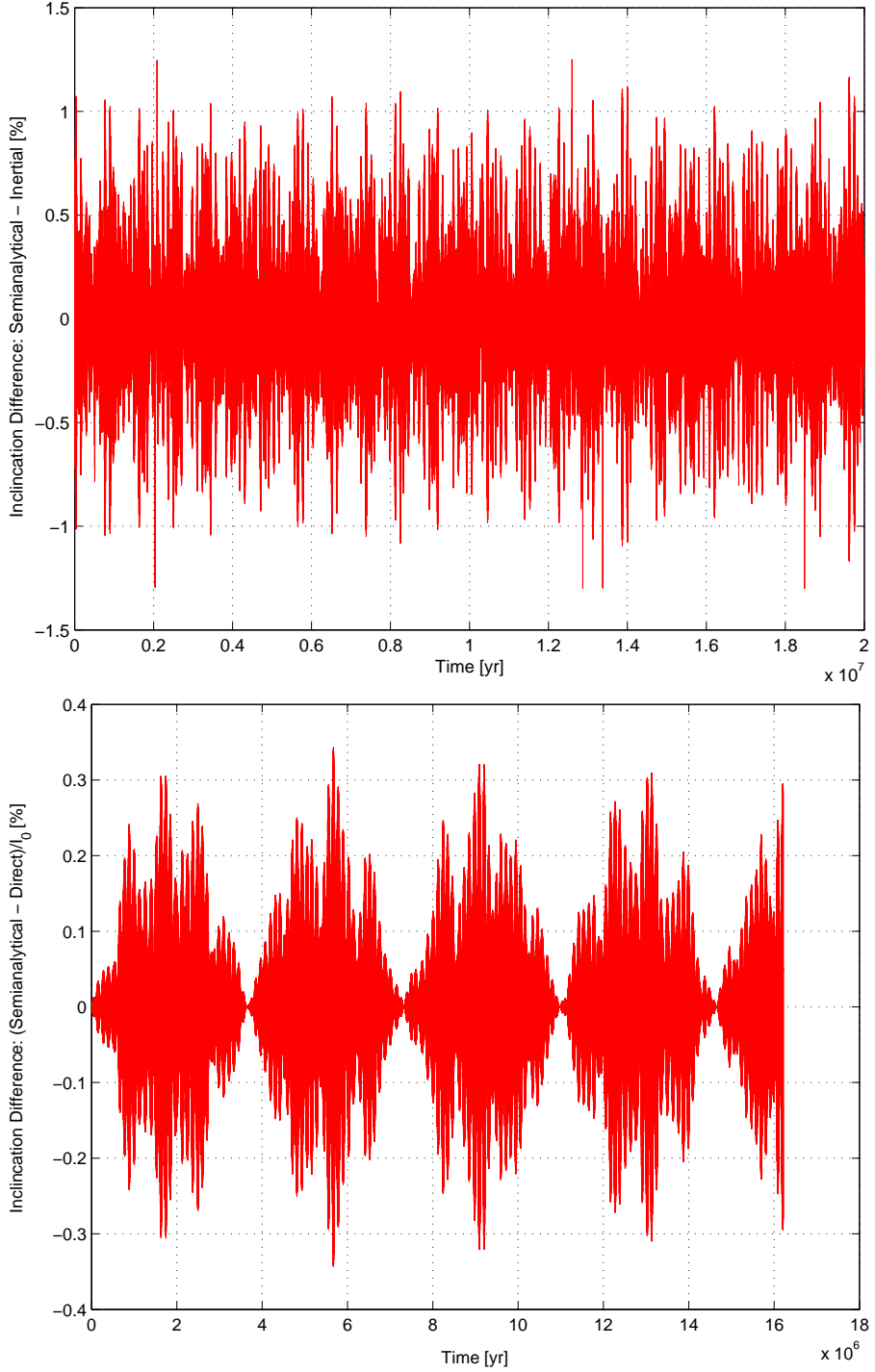


Figure 6: Comparison of the semianalytical model to a purely numerical integration. The plot shows the differences in inclination as predicted by the two models, normalized by the initial inclination. The top plot shows the case of the initial inclination $i_0 = 0.5$ deg. In this case, the difference between the two models stays within less than 1.3% for over 20M yr. The bottom plot depicts the case of $i_0 = 89$ deg. In this case, the difference between the two models stays within less than 0.3% for over 20M yr.

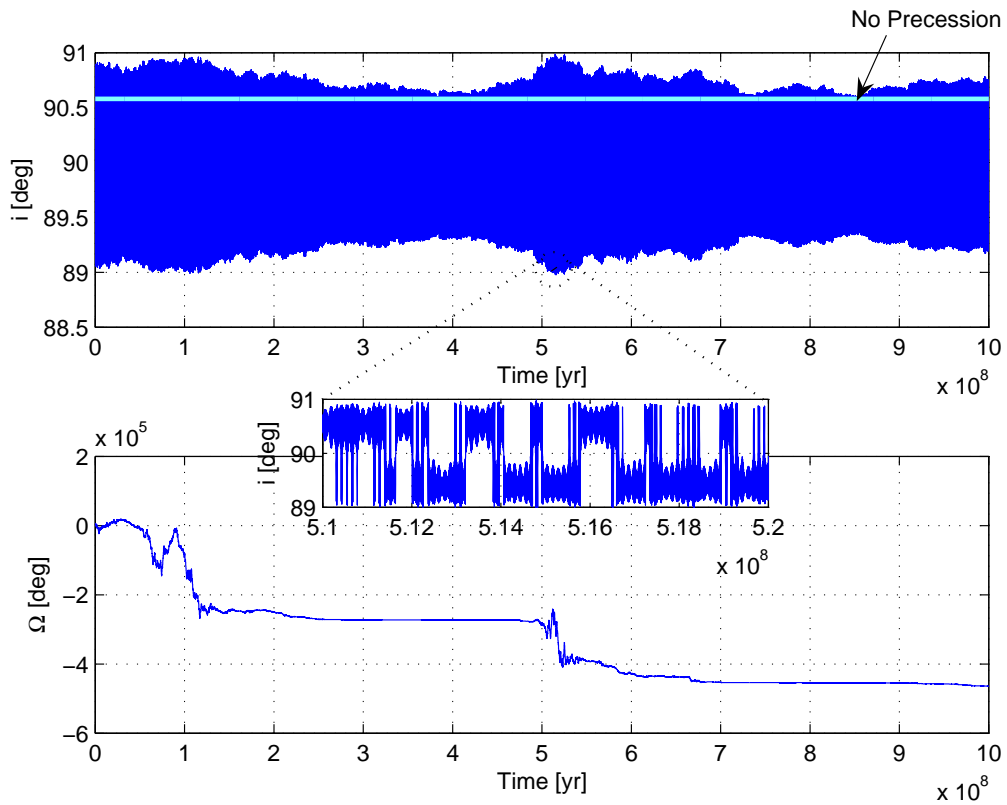


Figure 7: Evolution of the inclination and longitude of the node, for the initial conditions that entail maximal variations of the orbit inclination. The plot, obtained by integration of the semi-analytical model, demonstrates that inclination locking persists. However, when precession is neglected, the chaotic variations of the inclinations disappear, and the inclination remains frozen at its initial value.

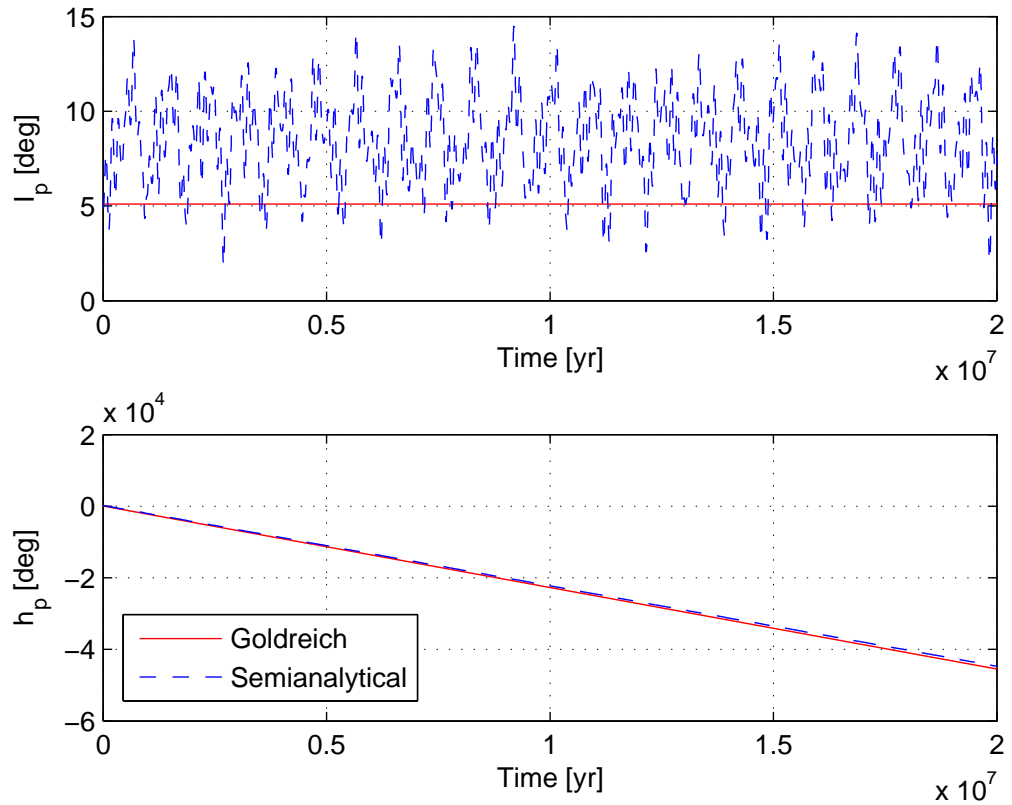


Figure 8: Preparation to comparison of the semianalytical model to Goldreich's model. In Goldreich's model, the Martian equator is assumed to precess uniformly, while the semianalytical model takes into account (via Colombo's equation) variations of the equinoctial precession.

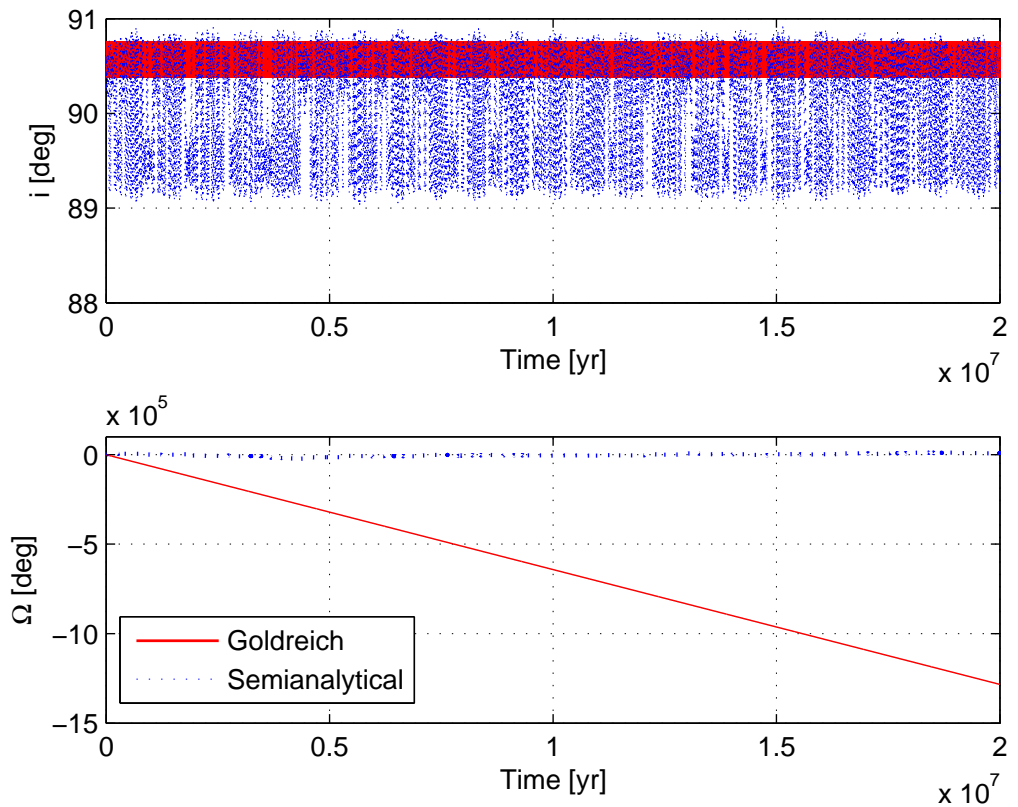


Figure 9: Comparison of the semianalytical model to Goldreich's model. Deimos' inclination in Goldreich's model remains tightly locked, while the semianalytical model reveals much larger variations of the satellite's inclination.